Experimental and finite element modal analysis of photovoltaic modules for the design of next-generation vehicle-integrated PV applications

Bin Luo [1,3,4,5,*], Simone Gallas [2,6,*], Cynthia Micallef [2,6], Jonathan Govaerts [3,4,5], Konstantinos Gryllias [2,6], Jef Poortmans [1,3,4,5]

[1]Department of Electrical Engineering (ESAT), KU Leuven, 3001 Heverlee, Belgium
[2]Department of Mechanical Engineering, KU Leuven, 3001 Heverlee, Belgium
[3]Imec, imo-imomec, Thor Park 8320, 3600 Genk, Belgium,
[4]Hasselt University, imo-imomec, Martelarenlaan 42, 3500 Hasselt, Belgium,
[5]EnergyVille, imo-imomec, Thor Park 8320, 3600 Genk, Belgium
[6]Flanders Make @ KU Leuven, Leuven, Belgium

[*]Corresponding author: Bin Luo (bin.luo@imec.be) and Simone Gallas (simone.gallas@kuleuven.be)

Abstract

Being different from terrestrial photovoltaic (PV), vibration response is critical to PV modules for vehicle applications, as dynamic loads lead to vibration responses in VIPV modules, which must be carefully considered during the structural design phase to prevent noise and fatigue failure. In this work, the experimental modal analysis on conventional glass-based and novel composite-based, lightweight PV module structures is investigated. First, the modal frequencies and mode shapes are determined by experimental modal analysis on different module structures with/without solar cell strings. Based on the experimental results, the solar cells have negligible influence on vibration response of glass-based PV panels, whereas their influence is non negligible for the considered lightweight panels. The lightweight panels show a higher number of modal frequencies within the 0–120 Hz range and greater amplification factors for these modes compared to the glass-glass modules. The experimental results are used to update a finite element model and quantify its accuracy for the prediction of modal frequencies and shapes. The sensitivity analysis, based on the numerical modal, suggests the significance of skin material properties, i.e., thickness, Young's modulus and density. The findings highlight the challenges of implementing lightweight structures for vehicle applications and provide a fundamental understanding of vibration performance for next-generation VIPV applications.

Key words: VIPV, lightweight modules, vibration response, modal analysis

1. Introduction

With a rapid growth of deployment in recent years, photovoltaic (PV) is foreseen to be one of the most significant and sustainable energy sources in the future [1], [2]. The concept of "integrated PV" combines different systems and PV to reduce the carbon footprint of the entire system. Examples include Building-integrated PV (BIPV) and Vehicle-integrated PV (VIPV). Considering massive CO_2 emission is induced by transportation activities [3], VIPV might be part of the solution to alleviate this.

Although current VIPV products already exist on the market [4], [5], with a main focus on integrating PV into the panoramic roof, the power density provided by such a "solar roof" is still limited (around 200 Wp/m^2) [6]. Therefore, to enhance the energy yield, the next

generation VIPV product should aim to maximize PV coverage across the entire surface of the car, including the hood, trunk, and even body panels [7]. Achieving high integration across vehicle surfaces requires lightweight PV modules to preserve aerodynamic efficiency and minimize the additional weight introduced by PV components. In this case, the weight of conventional glass-glass modules (weighing up to 20 kg/m^2) [8] is not negligible compared to the weight of an electric vehicle itself (weighing 1500-2200 kg) with a hypothetical area of 10 m^2 [9]. Thus, lightweight PV modules are imperative to be considered for the next generation VIPV applications.

Although there is lack of standards specifically for VIPV products, some safety qualifications have been proposed and conducted by different researchers [10], [11]. On the one hand, environmental stability remains significant for terrestrial PV applications, including thermo-mechanical, damp heat storage, UV stability. Previous studies have shown that thermo-mechanical and damp heat reliability is challenging for lightweight PV modules [12], [13], [14]. When the skin layer is replaced from glass to fiber reinforced polymers, the coefficient of thermal expansion and water vapor transmission rate have significant differences, which result in environmental reliability issues. On the other hand, impact and dynamic response (i.e. vibration behavior) also play an important role in vehicle applications, as noise, vibration and harshness (NVH) design significantly impact the user comfort [15] and the structural fatigue life. Over past years, prior studies have reported on the vibration behaviour of PV modules during transportation [16], [17] and under wind load with different mounting configurations [18]. However, to the knowledge of the authors, a comprehensive and fundamental analysis of the vibration behaviour between conventionally bulk glass-based modules and novel lightweight modules has not been reported yet.

The goal of this paper is to better understand and simulate the vibration behavior of the novel lightweight PV modules for an improved NVH design of the vehicle. Therefore, in this paper, the results of experimental modal analysis in a free preload-free constraint condition (also referred to as “free-free”) are presented to determine the dynamic properties (modal frequencies and mode shapes) of PV modules for vehicle applications. The modal frequencies and mode shapes are compared between glass-glass and lightweight (using glass-/carbon-fiber reinforced polymers as backsheet) modules. Under the assumption of small linear-elastic displacements, the vibration behavior can be conveniently synthetized in terms of modal frequencies, shapes and damping values. Therefore, to reach the above-mentioned goal, we propose an experimental and numerical modal analysis of conventionally bulk glass-based modules and novel lightweight modules.

2. Experimental section

2.1 Sample fabrication

The module structure consists of frontsheet, front encapsulant, solar cell with interconnections, back encapsulant and backsheet (shown in Figure 1 (a) and (d), marked as type “A”). Three module structures are fabricated in a small size (35×35 cm^2): namely (i) a conventional glass-glass (GG) module, (ii) a lightweight module with polyethylene terephthalate (PET) frontsheet-glass fiber reinforced polypropylene (GFPP) backsheet and (iii) a lightweight module with PET frontsheet-carbon fiber reinforced polypropylene (CFPP) backsheet module. To understand the influence of each PV component on the vibration

response of the PV module, module structures with only solar cells (w.o. interconnection, seen in Figure 1 (b) and (e), marked as type "B") and without any PV (w.o. solar cells and interconnections, shown in Figure 1 (c) and (f), marked as type "C") have been fabricated and tested for their modal features. Detailed sample fabrication process and module mass and thickness are described in Supplementary Information S1.

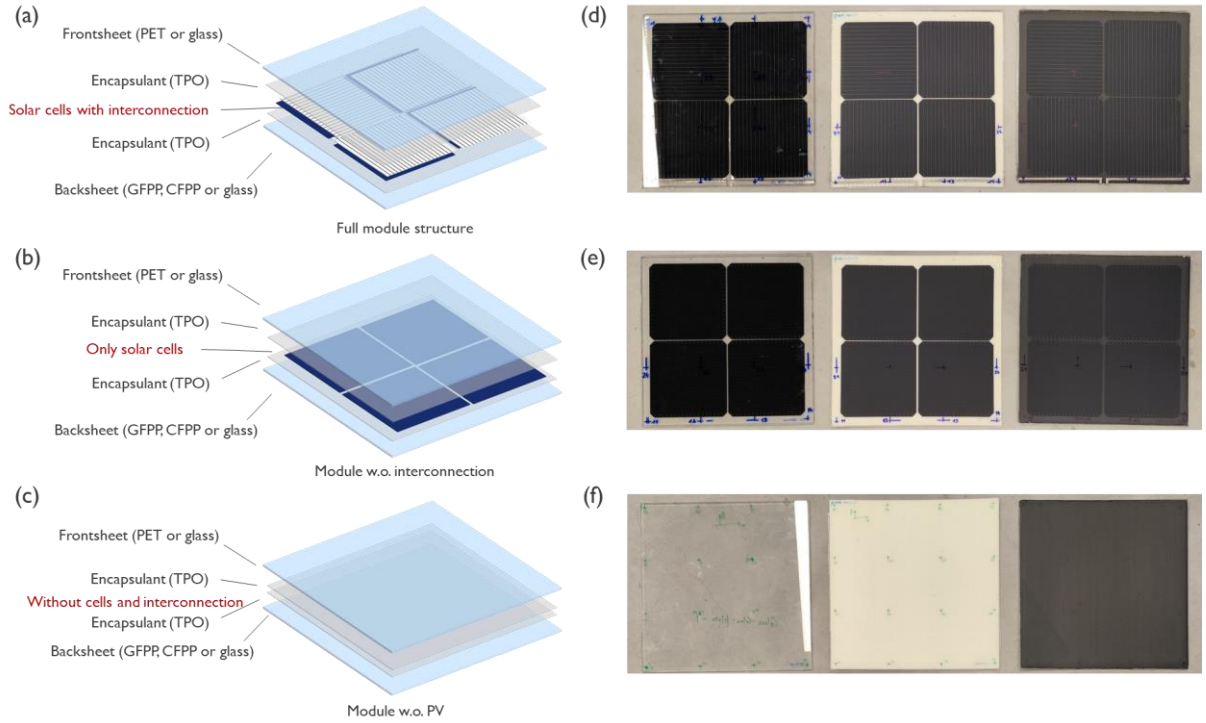

Figure 1. The schematic picture of PV module structures and sample images: (a) the full module structure (sample type A), (b) the module without interconnection (sample type B) and (c) the module without solar cell and interconnection (sample type C), (d)-(f) corresponding images to structures (a)-(c), each time showing left to right GG, PET-GFPP and PET-CFPP buildup.

2.2 Free vibration test

A regular 4 x 4 grid is marked on each sample to indicate the excitation locations, as illustrated in Figure 2 (a). With this type of grid, it is possible to distinguish at least the first 4-5 typical mode shapes of squared plates in free-free conditions. [19] The free pre-load and free constraint test condition is selected because of the expected low influence on the modal results, which is realized by hanging the samples with elastic bands. Three lightweight accelerometers (model PCB 352A24) are mounted on the rear side of the structure using beeswax, at the grid locations labelled as "11", "22" and "33" according to Figure 2 (a). An automatic hammer (model NV-TECH SAM1) is used to excite the sample sequentially at the grid points at the frontside, applying an excitation force that ranges between 0.34 and 3.30 N. In this range, the acceleration response is found to scale linearly with the excitation force. The frequency response functions (FRFs) between acceleration response and excitation force are measured per each of the 16 excitation locations. Details of data collection are described in Supplementary Information S2. The samples labelled as "GG-A-1", "GF-A-1" and "CF-A-1" are excited at each location of the grid, whereas symmetry is exploited for the other samples, which are only excited at the locations in the lower half of the grid. The experimental setup is shown in Figure 2 (b) and (c) for the sample "GF-A-1", as an example.

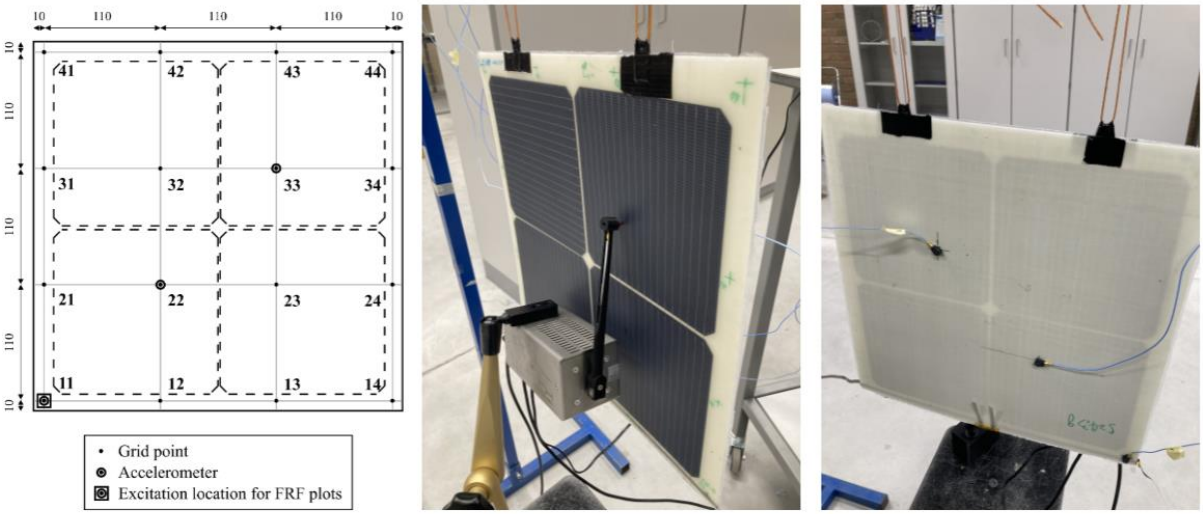

(a) Dimensions and grid (b) Front view (c) Back view

Figure 2. (a) The layout of excitation spots on each sample and position of accelerometers. (b) The front view of GF sample during experimental modal analysis, showing the mounting method and excitation position. (c) The back view of GF sample showing the position of accelerometers.

3. Finite element (FE) modeling

3.1 Finite element model and mesh

FE models are extensively used for prediction of structures' modal frequencies and modal shapes. After the initial investigation on the element type (details seen in Supportive Information S3), 3D elements are chosen to represent each layer with elimination of interconnections in the geometry (which will be discussed in Section 4.1). The 3D FE model is realized with Simcenter 3D integrated framework and solved with solution "103 - Real Eigenvalues" in NX Nastran. The parameters of this model are then analyzed and updated with the multi-disciplinary design optimization software HEEDS.

Table 1. Material properties used in the initial FE model

Material	Thickness [mm]	Young's modulus [MPa]	Density [kg/m^3]	Poisson factor [ ]
PET frontsheet	0.3*	2000*	1150*	0.29#[20]
Encapsulant	0.21 (GG), 0.55(other) *	45.8*	902*	0.26#[21]
Silicon	0.18*	170000#[22]	2329#[16]	0.28#[16]
Glass	3*	74000# [23]	2520*	0.24#[23]
GFPP	1.7*	11000# [24]	1495*	0.25#[25]
CFPP	1.25*	54000# [24]	1370*	0.25#[26]

* Measured

From literature

3.2 Material properties and constraints

The nominal properties used for the initial FE model are listed in Table 1. In the first approximation linear elastic isotropic material models are used. The thickness of each layer is measured with a confocal microscope over the sample cross-section. The Young's modulus of PET frontsheet and encapsulant was estimated as the storage modulus, which is measured using a Dynamic Mechanical Analysis (DMA) in tension mode at an oscillation frequency of 1 Hz and temperature of 23 °C. The densities of PET, encapsulant, GFPP and CFPP are measured. The density of glass is instead tuned in order to match the total weight of the samples. All the remaining material properties are taken from literature. With these assumptions, the total thickness and weight of the modelled samples matched the real samples with a maximum percentage error of 1%. No structural constraint was applied to represent the experimental free-free conditions.

4. Results and discussion

4.1 Experimental modal analysis

The modal features of each sample are estimated on the base of the FRF that are measured in the free vibration test. The FRF with excitation and response at the grid point "11" is shown as an example in Figure 3 (a). Per each frequency, it illustrates the amplitude of the acceleration response at point "11" resulting from a unit impulse excitation applied at the same point "11". In such a plot, the peaks indicate vibrational modes, showing the frequencies at which the system naturally resonates. The repeatability of the measurement is proven to be good for the 3 samples tested. Four vibration modes are found in the measurement range of 0-500 Hz for GG modules, corresponding to the "torsion", "saddle", "central" and "diagonal" modes at 177.7, 275.9, 312.6 and 416.9 Hz respectively. These modal shapes are shown in Figure 4. Interestingly, the "saddle" mode is not visible in the FRF of Figure 3 because of its very limited participation factor, but is suggested by the Polymax algorithm within Simcenter Testlab, which is used to estimate the modal features from the experimental data. More details on the estimation method can be found in Supportive Information S2. In this mode, half of the grid points, among which the accelerometers points (along the diagonal), are located in the proximity of nodal points, where the modal displacements are almost zero. When eliminating solar cells and interconnections, the modal frequencies do not change significantly (Figure 3 (b)), which suggests that PV has a minor impact on vibration response for the GG structure. This aligns with a prior reported study that solar cells and interconnections have negligible effects on the module stiffness for a full-size module, and therefore can be eliminated in FEM for simplifications for full size GG modules [27]. However, according to the scaling law [28], an increase in module size significantly reduces the modal frequencies.

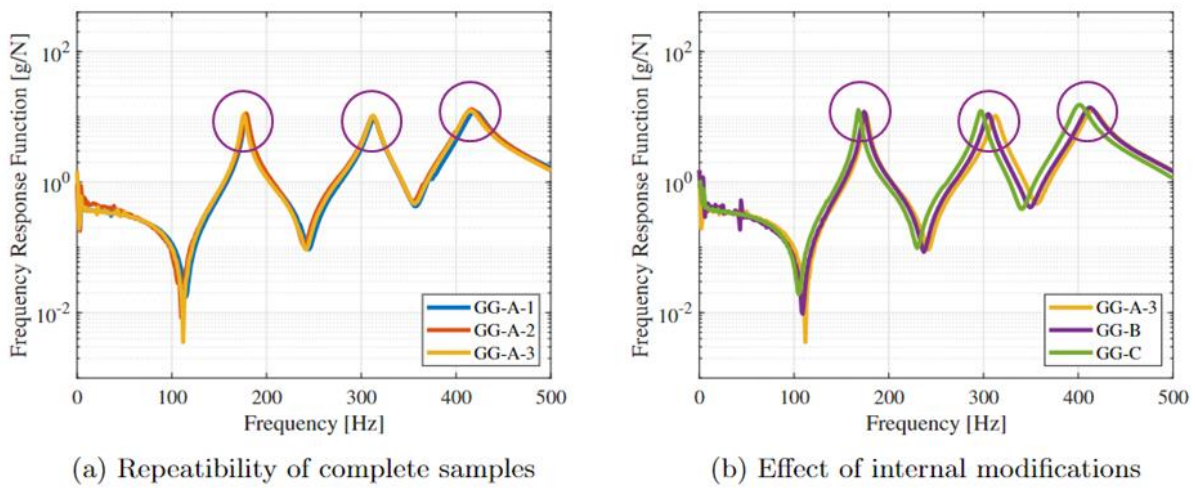

Figure 3. Measured FRFs of (a) full GG modules and (b) GG modules w./w.o. PV and interconnections. Excitation and response are both at grid point "11" (Figure 2). Peaks are marked.

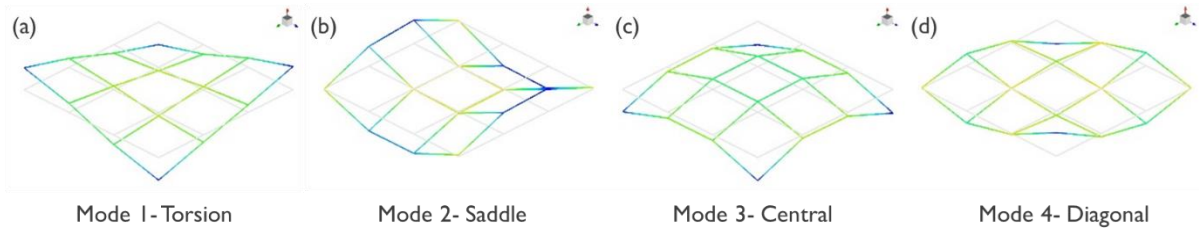

Figure 4. Experimental modal shapes of full GG modules for type A.

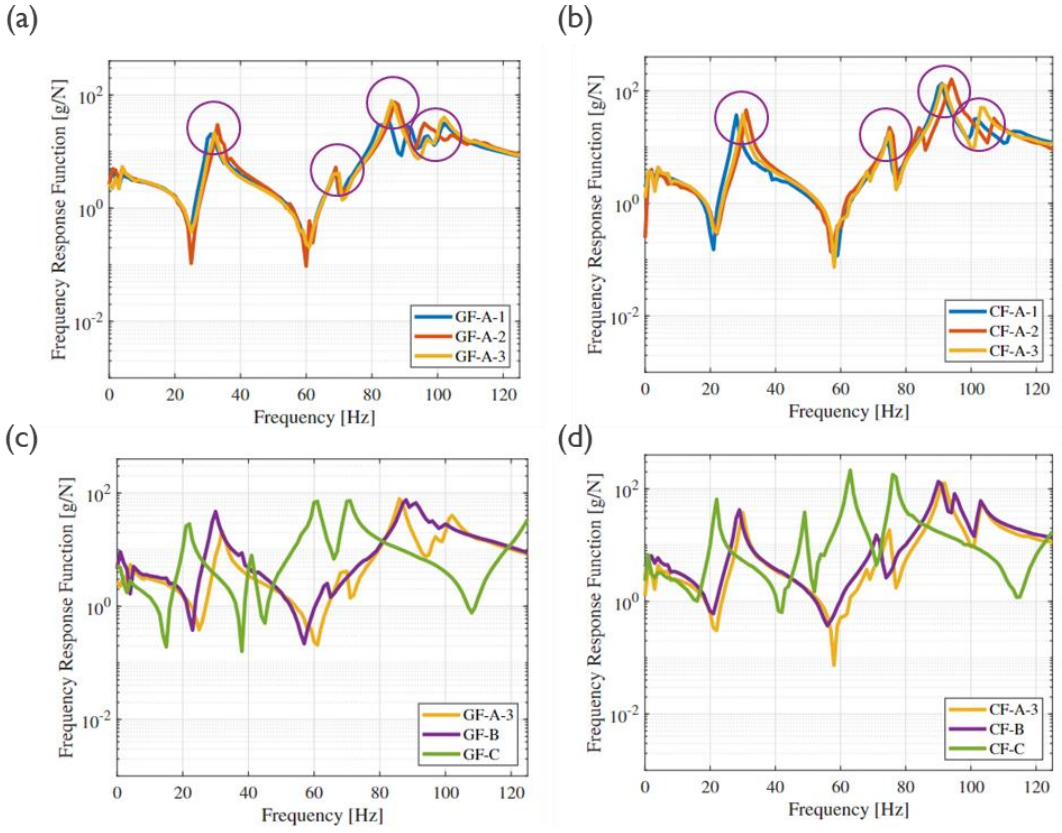

Figure 5. Measured FRFs of (a) full GFPP modules, (b) full CFPP modules, (c) and (d) GFPP and CFPP modules w./w.o. PV and interconnections. Excitation and response are both at grid point "11" (Figure 2). Peaks are marked.

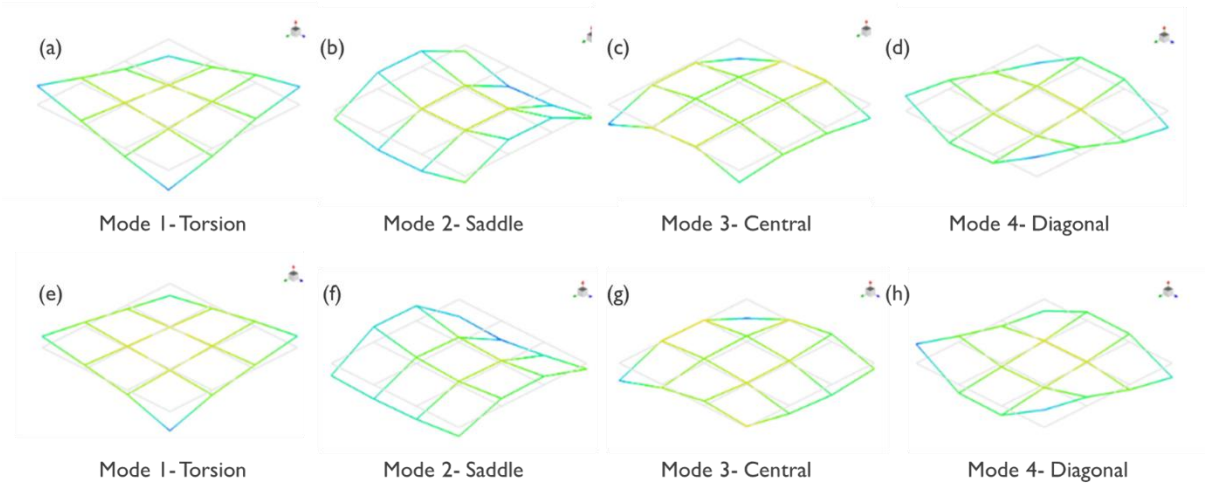

Figure 6. Experimental mode shapes of (a)-(d) GFPP modules (e)-(h) CFPP modules for type A

Next, the modal features of GFPP and CFPP modules are estimated. The modes that are observed for GG modules are now shifted to significantly lower frequencies and can be found in the range 0-120 Hz, which coincides with the typical range of frequencies excited due to vehicle-road interaction [29]. As shown in Figure 5 (a) and (b), four vibration modes are detected, corresponding to the "torsion" (32 Hz), "saddle" (72 Hz), "central" (91 Hz) and "diagonal" (104 Hz) modes as shown in Figure 6. The respective modes for GFPP and CFPP are very similar in modal frequency due to similar geometry. Compared to GG modules, the modal density (i.e. the number of modes within a certain frequency range) and the modal amplification (i.e. the height of the peaks in the FRFs) are both higher. These observations indicate that within the same frequency range, the lightweight PV modules are more prone to resonance issues. It is noteworthy that the repeatability of the measurement for lightweight modules is also limited, which can be observed from side peaks and noise in Figure 5 (a) and (b). This might be due to the shift in position of the bussing ribbons that slightly alter the geometry of each module, which results from uncertainties of manually fabricated lightweight modules, as demonstrated in Figure S1. Module structures without interconnection and/or solar cells are also tested. It is found that solar cells have a significant impact on the vibration response by increasing the modal frequencies, while the effect of interconnections is limited compared to cells, as shown in Figure 5 (c) and (d). This indicates that FE modeling for lightweight modules should include solar cells but can neglect the interconnection (but not the bussing ribbons).

The modal features for all the samples are summarized in Table 2. The first column contains the average of the modal frequencies among the full samples, and the second column contains the standard deviation. The third and fourth columns indicate the relative variations of modal frequencies due to the removal of the interconnections and the solar cells

respectively. The comparison between these modal frequencies is only valid when the modal shapes are similar. In this paper, two modal shapes are considered similar when their Modal Assurance Criterion (MAC) value is higher than 0.5. [30] The modal damping values are shown in Supplementary Information Table S3. While the modal frequencies show evident patterns with respect to the sample types, the modal damping values are very scattered and more difficult to interpret. It seems that the modal damping values are more sensitive to the manufacturing and testing uncertainties.

Table 2. The modal features of GG, GF and CF samples

		Modal frequency			
Sample	Mode	Average value of full module structure (type A) [Hz]	Std. dev. of module structure (type A) [%]	Freq. change of structure of no interconnection (type B vs type A) [%]	Freq. change of structure of no solar cells (type C vs type A) [%]
GG	1-Torsion	178	0.7	-1.81	-5.39
	2-Saddle	276	0.57	-2.93	-6.27
	3-Central	313	0.12	-2.41	-4.86
	4-Diagonal	417	0.50	-0.81	-3.04
GF	1-Torsion	33	1.69	-8.87	-34.21
	2-Saddle	70	1.29	-8.33	-41.65
	3-Central	88	1.36	3.62	-30.76
	4-Diagonal	103	0.94	-2.73	N.A.*
CF	1-Torsion	30	5.28	-3.26	-25.24
	2-Saddle	74	1.50	-3.79	-34.40
	3-Central	93	1.18	-2.88	-32.30
	4-Diagonal	105	1.33	-2.10	N.A. *

*Note: the modal shape for type C is significantly different (MAC < 0.5) from the modal shape obtained in type A, therefore, the comparison between frequencies each mode is not valid.

4.2 Numerical sensitivity analysis

In the second step, the modal frequencies and shapes are predicted with the FE model. The model is used for a sensitivity analysis to understand the impact of design parameters such as layer thickness or the material properties, on modal frequencies. The sensitivity is defined as the percentage variation of modal frequencies due to a +10% variation of a certain design parameter with respect to its nominal value shown in Table 1. As illustrated in Figure 7 (a), when considering only one design parameter for the GG sample, the sensitivities are very similar for all modes. It can be observed that the highest sensitivities regard the front- and backsheets, in terms of thickness, Poisson's ratio and Young's modulus. The sheets' sensitivities for the glass material properties case are the same for front and back sheets due to the symmetric construction. Then, the sensitivities are averaged among the modes and

compared among the different types of samples, as shown in Figure 7 (b). Here, the sensitivity related to backsheet properties is more dominant than the frontsheet for lightweight modules. The sensitivity related to solar cells is higher for lightweight modules, compared to the glass-glass modules, which confirms that solar cells are essential to be considered for structural analysis of lightweight modules. These findings provide critical insights for optimizing lightweight PV module designs.

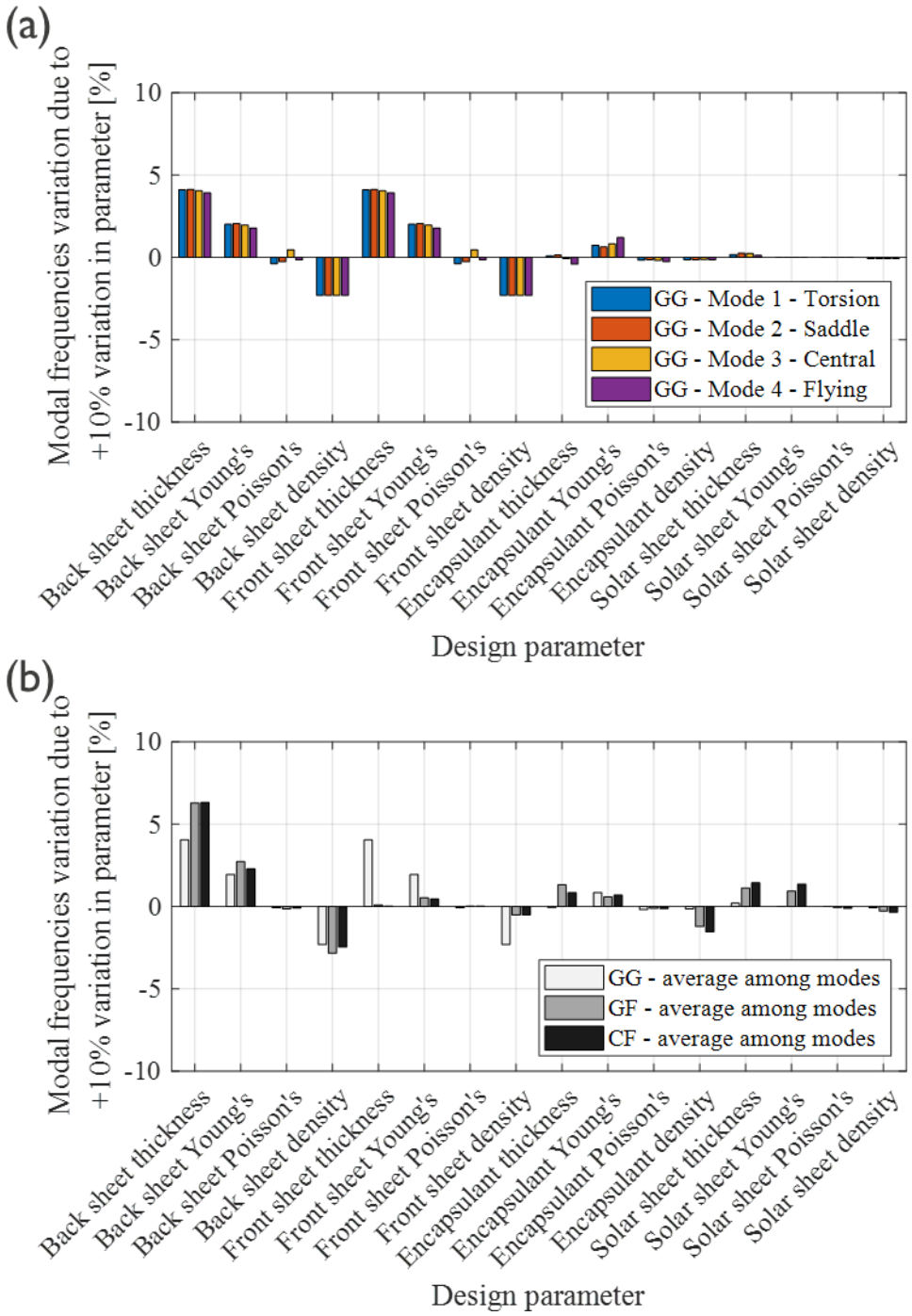

Figure 7: Sensitivities around nominal design parameters: (a) for all modes of the GG sample. (b) For the average modes of the GG, GF and CF samples.

4.3 Correlation and model update

On one hand, the sensitivity analysis supports the designer when tuning the modal response of the PV panel. On the other hand, this analysis indicates which parameters should be updated primarily in order to have a more accurate simulation of the modal frequencies.

Therefore, the numerical results are then correlated to the experimental ones, to verify the accuracy of the initial FE model and to improve it with the update of its material parameters. The correlation of the modes is based on the similarity of the modal shapes, which is also quantified with the MAC [30]. Each simulated mode is paired to an experimental mode with a MAC value always higher than 0.5. In this way, 4 mode pairs are obtained for each sample case.

Per each mode pair, the percentage error between the experimental and simulated modal frequency is an indicator of model accuracy. These errors are synthesized in the root mean square objective function:

$$\epsilon(\boldsymbol{p}) = \sqrt{\frac{1}{n_m}\sum_{k=1}^{n_m}\left[\frac{\mathrm{f}_k^{sim}(\boldsymbol{p}) - \mathrm{f}_k^{exp}}{\mathrm{f}_k^{exp}}\right]^2}$$

Where n_m is the number of the paired modes, $\boldsymbol{p}$ is the vector of the design parameters, f_k^{exp} is the k-th experimental modal frequency of the full sample (sample type "A") and f_k^{sim} is the k-th simulated one. The objective function $\epsilon(\boldsymbol{p})$ is minimized with respect to certain design parameters with the SHERPA optimization routine [31], with maximum number of evaluations set to 50.

Thicknesses and densities are not considered as design parameters to be updated because they are measured with simple and well-established methods. Among the other design parameters, the most sensitive ones are selected for the model update. After this selection, the conditioning of the identification problem is verified. In all cases, the condition number of the sensitivity matrix lies between 1 and 10^3, confirming that the selected parameters can be identified [32].

Within the optimization routine, upper and lower boundaries are applied to the selected parameters, as percentage of the nominal values. The lower boundary is 50% of the nominal value and the upper boundary is 150%. For the GG case, the update of the selected parameters results in a reduction of the objective function $\epsilon(\boldsymbol{p})$ from 3.56% to 0.63%, as shown in Table 3.

Table 3. Parameters variation and modal frequency errors for the GG modules

		GG	
		Initial	Final
Design parameters	Front and back Young's modulus [GPa]	74.00	81.40
	Front and back Poisson's ratio [ ]	0.24	0.25
	Encapsulant Young's modulus [MPa]	45.80	44.88

Modal frequency errors	Mode 1 - Torsion	-3.83%	-0.32%
	Mode 2 - Saddle	-4.29%	-0.60%
	Mode 3 - Central	-2.86%	1.07%
	Mode 4 - Diagonal	3.07%	0.05%
Objective function	$\epsilon(\boldsymbol{p})$	3.56%	0.63%

When a similar optimization procedure is repeated for the lightweight samples, the objective function cannot be reduced below 16.64% and the parameters values approach the assumed boundaries, indicating an inaccurate assumption in the structure of the FE models as shown in Table 6. In further work, it is necessary to understand the cause of uncertainty for the lightweight model, which could be the material model of composite backsheets.

Table 6. Parameters variation and modal frequency errors for the lightweight modules with isotropic material model

		GF-A		CF-A	
		Initial	Final	Initial	Final
Design parameters	Front Young's modulus [GPa]	2.00	2.78	2.00	1.00
	Back Young's modulus [GPa]	11.0	9.57	54.00	27.00
	Back Poisson's ratio [ ]	0.25	0.375	0.25	0.375
	Encapsulant Young's [MPa]	45.8	68.2	45.8	22.9
Modal frequency errors	Mode 1 - Torsion	33.13%	28.11%	88.28%	45.06%
	Mode 2 - Saddle	-10.01%	-11.60%	7.08%	-18.11%
	Mode 3 - Central	-17.21%	-13.33%	-1.85%	-23.63%
	Mode 4 - Diagonal	3.79%	2.13%	29.06%	-1.09%
Objective function	$\epsilon(\boldsymbol{p})$	19.42%	16.64%	46.61%	27.01%

5. Conclusions and outlook

In this work, experimental and numerical modal analysis are presented on conventional glass-glass and novel lightweight PV modules targeting VIPV applications.

Through experimental modal analysis, it is demonstrated that the modal density and the modal amplification factors of lightweight PV modules are higher than those for traditional glass modules. PV strings have a limited impact on changing modal features for a GG structure, whereas they can significantly affect modal features for lightweight structures. The experimental analysis also shows that the effect of manufacturing tolerances on modal frequencies is limited for glass-glass modules but more prominent for lightweight modules, presenting a challenge for lightweight modules in VIPV applications.

The numerical modal analysis shows a more accurate prediction of modal frequencies for glass-glass modules compared to the lightweight modules. The sensitivity analysis confirms that PV strings have a higher impact on modal frequencies for lightweight modules compared to glass-glass modules. All the correlations are improved by updating the most sensitive and uncertain material properties. The improvement results in more accurate correlations for glass-glass modules compared to lightweight modules. However, it is challenging to obtain

good correlation between experimental and simulated modal frequencies for lightweight modules (objective function >16.64%), where the updated parameters might be unrealistic (by varying up to 50% Young's modulus of frontsheet and backsheet). Further investigation is required to improve the FE model specifically for lightweight modules.

This study bridges the research gap by comparing the vibration responses of conventional glass-based modules with those of novel lightweight modules. On the one hand, it experimentally highlights some of the new NVH challenges related to the introduction of novel lightweight PV modules. On the other hand, the paper investigates the accuracy of a FE model-based approach, which can be used for a product in actual size and with realistic mounting system. For further studies, the actual module size and mounting system should be taken into account to obtain accurate modal features for each specific case. Modal frequencies might increase with added constraints and decrease with larger modules sizes. Depending on the VIPV design, the impact of VIPV dimensions and form on modal features should be also investigated in the future study. Furthermore, as a next step, random vibration and shock testing based on ISO 16750 should be carried out using the actual design and mounting system. The current study approach could be used to the NVH challenges in the design of future generation VIPV modules.

Acknowledgements
The authors gratefully acknowledge the Flemish government for its financial support through the funded ICON projects "SNRoof" (HBC.2020.2379) and related project partners, as well as the European Union's Horizon 2020 Programme for research, technological development and demonstration for funding part of this work under Grant Agreement no. 857793 (HighLite). The authors also would like to acknowledge the partial funding by the Kuwait Foundation for the advancement of Sciences under project number P115-15EE-01.

Conflict of interests
The authors declare no known conflict of interest.

Data availability statement
The data that support the findings of this study are available from the corresponding authors upon reasonable request.

Author contribution statement
B.L. and S.G. contributed equally to this work. B.L., S.G. and K.G. conceived the idea of this work. B.L. coordinated the work, fabricated testing samples, measured material properties, prepared manuscript and figures. S.G. conducted experimental modal analysis and finite element analysis, prepared manuscript and figures. C.M. carried out experimental modal analysis. J.G., K.G. and J.P. contributed conceptual ideas, results interpretation and supervised the work. All authors made valuable comments and contributed to the manuscript.

References

[1] Nancy M. Haegel et al., “Terawatt-scale photovoltaics: Transform global energy”. *Science*, 364,836-838(2019).DOI:10.1126/science.aaw1845

[2] Nancy M. Haegel et al. , “Photovoltaics at multi-terawatt scale: Waiting is not an option”. *Science*, 380, 39-42(2023).DOI:10.1126/science.adf6957

[3] O. US EPA, “Global Greenhouse Gas Overview.” Accessed: May 22, 2024. [Online]. Available: https://www.epa.gov/ghgemissions/global-greenhouse-gas-overview

[4] “2024 Toyota Prius Prime Specs | Toyota.com.” Accessed: Nov. 29, 2023. [Online]. Available: https://www.toyota.com/priusprime/2024/features/

[5] “Hyundai launches first car with solar roof charging system.” Accessed: Jun. 03, 2023. [Online]. Available: https://www.hyundai.news/eu/articles/press-releases/hyundai launches-first-car-with-solar-roof-charging-system.html

[6] M. Yamazaki, "VIPV Japan VIPV R&D activities in NEDO," in *PVinMotion 2023*, ’s-Hertogenbosch, the Netherlands, Feb. 15-17, 2023

[7] M. Heinrich et al., “Potential and Challenges of Vehicle Integrated Photovoltaics for Passenger Cars,” *37th Eur. Photovolt. Sol. Energy Conf. Exhib.* 1695-1700, p. 6 pages, 6119 kb, 2020, doi: 10.4229/EUPVSEC20202020-6DO.11.1.

[8] A. C. Martins, V. Chapuis, A. Virtuani, and C. Ballif, “Ultra-Lightweight PV module design for Building Integrated Photovoltaics,” in *2017 IEEE 44th PVSC*, Jun. 2017, pp. 2104–2108. doi: 10.1109/PVSC.2017.8366791.

[9] N. Patel, K. Bittkau, B. E. Pieters, E. Sovetkin, K. Ding, and A. Reinders, “Impact of Additional PV Weight on the Energy Consumption of Electric Vehicles With Onboard PV,” *IEEE J. Photovolt.*, vol. 14, no. 2, pp. 319–329, Mar. 2024, doi: 10.1109/JPHOTOV.2024.3359446.

[10] J. Markert, C. Kutter, B. Newman, P. Gebhardt and M. Heinrich, “Proposal for a Safety Qualification Program for Vehicle-Integrated PV Modules.”, *Sustainability* 2021, 13, 13341. Accessed: May 22, 2024. [Online]. Available: https://www.mdpi.com/2071-1050/13/23/13341

[11] “IEC develops standards for vehicle-integrated photovoltaics,” pv magazine International. Accessed: May 22, 2024. [Online]. Available: https://www.pv-magazine.com/2024/04/30/iec-develops-standards-for-vehicle-integrated-photovoltaics/

[12] B. Luo et al., “Development and thermo-mechanical reliability assessment of fiber reinforced polymers in lightweight PV modules towards vehicle-integrated photovoltaics,” *Sol. Energy Mater. Sol. Cells*, vol. 259, p. 112455, 2023, doi: https://doi.org/10.1016/j.solmat.2023.112455.

[13] J. Govaerts et al., “Development and testing of light-weight PV modules based on glass-fibre reinforcement,” *EPJ Photovolt.*, vol. 13, p. 13, 2022, doi: 10.1051/epjpv/2022007.

[14] B. Luo et al., “Encapsulation strategies for mechanical impact and damp heat reliability improvement of lightweight photovoltaic modules towards vehicle-integrated applications.” *Sol. Energy Mater. Sol. Cells*, vol. 273, p. 112932, 2024, doi: https://doi.org/10.1016/j.solmat.2024.112932

[15] S. Young, “Vehicle NVH Development Process and Technologies,” *21st International Congress on Sound and Vibration*, Beijing, China, 2014.

[16] U. Desai et al., “Prediction of vibration induced damage in photovoltaic modules during transportation: finite element model and field study.” *Eng. Res. Express* 3 045045, doi: 10.1088/2631-8695/ac3d12

[17] M. Köntges et al., “Impact of transportation on silicon wafer-based photovoltaic modules,” *Prog. Photovolt. Res. Appl.*, vol. 24, p. n/a-n/a, Mar. 2016, doi: 10.1002/pip.2768.
[18] B. Nan et al., “Wind Load and Wind-Induced Vibration of Photovoltaic Supports: A Review,” *Sustainability*, vol. 16, no. 6, Art. no. 6, Jan. 2024, doi: 10.3390/su16062551.
[19] I. Senjanović et al., “An Analytical Solution to Free Rectangular Plate Natural Vibrations by Beam Modes – Ordinary and Missing Plate Modes,” *Trans. FAMENA*, vol. 40, no. 3, pp. 1–18, Nov. 2016, doi: 10.21278/TOF.40301.
[20] O. Hasan, A. F. M. Arif, and M. U. Siddiqui, “Finite Element Modeling, Analysis, and Life Prediction of Photovoltaic Modules,” *J. Sol. Energy Eng.*, vol. 136, no. 021022, Dec. 2013, doi: 10.1115/1.4026037.
[21] A. Beinert et al., “FEM-Based Development of Novel Back-Contact PV Modules with Ultra-Thin Solar Cells.” *33rd Eur. Photovolt. Sol. Energy Conf. Exhib*., Amsterdam, the Netherlands, 2017. doi: 10.4229/EUPVSEC20172017-1CO.1.2.
[22] N. Klasen et al., “FEM simulation of deformations in strings of shingled solar cells subjected to mechanical reliability testing,” presented at the *INTERNATIONAL SYMPOSIUM ON GREEN AND SUSTAINABLE TECHNOLOGY (ISGST2019)*, Perak, Malaysia, 2019, p. 020016. doi: 10.1063/1.5125881.
[23] A. J. Beinert et al., “Thermomechanical Design Rules for the Development of Photovoltaic Modules.” PhD Dissertation, Karlsruher Institut für Technologie, Accessed: May 23, 2024. [Online]. Available: https://publikationen.bibliothek.kit.edu/1000142510
[24] B. Breukers, "Reliability assessment and improvement of lightweight photovoltaic modules for vehicle integration", 2022 KU Leuven, Master Thesis
[25] Y. Xue et al., “Design and multi□objective optimization of the bumper beams prepared in long glass fiber□reinforced polypropylene.” *Polymer Composites*. 2021; 42: 2933–2947. doi: https://doi.org/10.1002/pc.26026
[26] M. Hashimoto et al., “Prediction of tensile strength of discontinuous carbon fiber/polypropylene composite with fiber orientation distribution,” *Compos. Part Appl. Sci. Manuf.*, vol. 43, no. 10, pp. 1791–1799, Oct. 2012, doi: 10.1016/j.compositesa.2012.05.006.
[27] M. Assmus et al., ″Measurement and simulation of vibrations of PV□modules induced by dynamic mechanical loads.″ *Prog. Photovolt: Res. Appl.*, 19: 688-694. doi.org/10.1002/pip.1087
[28] P. Singhatanadgid and A. N. Songkhla. “An experimental investigation into the use of scaling laws for predicting vibration responses of rectangular thin plates”, *J. Sound Vib.*, vol 311, no. 1-2, pp. 314-327, 2008. doi.org/10.1016/j.jsv.2007.09.006.
[29] ISO 16750, “Road vehicles — Environmental conditions and testing for electrical and electronic equipment,” International Organization for Standardization, 2023
[30] M. Pastor, M. Binda, and T. Harčarik, “Modal Assurance Criterion,” *Procedia Eng.*, vol. 48, pp. 543–548, Jan. 2012, doi: 10.1016/j.proeng.2012.09.551.
[31] “SHERPA.” Accessed: May 23, 2024. [Online]. Available: https://www.redcedartech.com/solutions/heeds-software/efficient-search/9-solutions/214-sherpa
[32] T. Lauwagie, “Vibration-Based Methods for the Identification of the Elastic Properties of Layered Materials.” KU Leuven, PhD Dissertation, 2005